# Finite-Element Application to Rocket Nozzle Aeroelasticity

D. R. Mason*
*Morton Thiokol Inc., Brigham City, Utah*
and
P. T. Blotter†
*Utah State University, Logan, Utah*

**The trend in rocket technology is toward thinner, larger expansion ratios and more flexible exit cones. Hence, susceptibility to aerodynamically induced flutter has been and is a concern to both designer and analyst. The objective of this investigation is to develop an analytical tool for treating the aeroelastic stability of thin, truncated conical shells subjected to internal supersonic flow, with particular application to rocket nozzle structures. Stiffness, mass, and damping matrices are derived for an axisymmetric conical shell frustum finite element. The matrix equation of motion for a prescribed circumferential harmonic is developed and an eigenproblem formed from which flutter instability is deduced by tracking complex eigenvalue part variation with increasing dynamic pressure. Several check problems are considered to validate the various aspects of the analytics and computer code. Following this, the flutter analysis of a gas-deployed skirt, a typical rocket nozzle element, is presented to illustrate its application to rocket nozzle hardware. For this particular case, the analytical results indicate flutter at a motor chamber pressure well above the operating chamber pressure.**

## Nomenclature

| | |
|---|---|
| $[a],[b]$ | = element aerodynamic damping and stiffness matrices, respectively |
| $A$ | = area |
| $A/A^*$ | = expansion ratio (nozzle area/nozzle throat area) |
| $[A],[B]$ | = system aerodynamic damping and stiffness matrices, respectively |
| $E$ | = modulus of elasticity |
| $h$ | = shell thickness |
| $[I]$ | = identity matrix |
| $[m],[k],[kg]$ | = element mass, stiffness, and geometric stiffness matrices, respectively |
| $M$ | = Mach number |
| $[M],[K],[Kg]$ | = system mass, stiffness, and geometric stiffness matrices, respectively |
| $n$ | = number of circumferential waves |
| $[N]$ | = shape function matrix |
| $P$ | = pressure |
| $q,Q$ | = generalized displacement, force |
| $r$ | = radius |
| $R$ | = gas constant |
| $s$ | = length parameter |
| $t$ | = time |
| $T$ | = temperature |
| $\mathfrak{I}$ | = kinetic energy |
| $u,v,w$ | = neutral surface displacements (Fig. 1) |
| $U,V,W,\psi$ | = nodal displacements (Fig. 1) |
| $u,u_i,u_g$ | = strain energies |
| $V$ | = volume |
| $v$ | = gas velocity |
| $w$ | = work of aerodynamic forces |
| $\alpha$ | = damping factor |
| $\beta$ | = $\sqrt{M^2-1}$ |
| $\gamma$ | = specific heat |
| $\epsilon$ | = strain |
| $\theta,\phi$ | = angular parameters (Fig. 1) |
| $\lambda$ | = complex eigenvalue $=\alpha+i\omega$ |
| $\nu$ | = Poisson's ratio |
| $\xi,\eta$ | = nondimensional length parameters ($\xi=s/1$, $\eta=\xi-\frac{1}{2}$) |
| $\rho$ | = gas density |
| $\rho_s$ | = shell density |
| $\sigma$ | = stress |
| $\omega$ | = circular frequency |

*Superscripts*

| | |
|---|---|
| $(\dot{})$ | = differentiation with respect to $t$ (e.g., $\dot{u}=du/dt$, $\ddot{u}=d^2u/dt^2$) |
| $()'$ | = differentiation with respect to $s$ (e.g., $u'=du/ds$) |

*Subscripts*

| | |
|---|---|
| $c$ | = chamber properties |
| $i,j$ | = nodal or local quantities |
| $n$ | = $n$th harmonic |
| $\infty$ | = freestream properties |

Received July 31, 1985; revision received March 7, 1986.


*Supervisor—Dynamics, Wasatch Division. Graduate Student, Department of Mechanical Engineering, Utah State University. Associate Fellow AIAA.
†Professor, Department of Mechanical Engineering.

## Background

AERODYNAMICALLY induced flutter of rocket nozzle exit cones has been a topic of interest and concern since the 1960s. The trend in rocket technology is toward larger expansion ratio and thinner, and more flexible exit cones which, from the standpoint of flutter, exceed both the current experience base and analytical capabilities.

The typical situation for a rocket nozzle exit cone approximates one of internal supersonic flow through a truncated conical shell supported in some fashion at the smaller diameter while free at the larger. Many upper-stage rocket motors have exit cones with large expansion ratios ($A/A^*=150{:}1$ or greater). Often these high expansion ratios are achieved by using extendible (movable) exit cones and gas-deployed skirts. These structures are potentially susceptible to flutter induced by the flow of high-Mach-number exhaust gases.

A large body of information concerning panel flutter research and testing currently exists dating from the 1950s to the present. Detailed research has been reported for flat

panels, while less information is available for cylindrical shells. During the 1970s, investigators extended their efforts to conical shell aeroelasticity. Dixon and Hudson[1,2] published thorough analytical studies of conical shell vibration, buckling, and flutter. Miserentino and Dixon[3] performed flutter testing on a truncated conical shell exposed to external supersonic airflow and internal pressure. Also of interest is the study of Shulman,[4] the earliest treatment of conical shell aeroelasticity found. Ueda and Kobayashi,[5] Bismarck-Nasr and Costa-Savio,[6] and Sunder et al.[7] have recently treated conical shell flutter via finite element techniques. These investigators considered only the simply supported conical shell with external supersonic flow which approximates a missile nose cone situation.

Documented instances of rocket nozzle failures due to flutter are few. Davidson and Gutsfield[8] reported flutter during a cloth nozzle extension test. In the mid-1970s, Thiokol Corporation conducted several subscale motor test firings with fabric exit cones which experienced failures attributed to flutter. These latter failures led to subscale cold-flow flutter tests wherein flutter was induced in two instances during the test series by reducing fabric axial tension while increasing aerodynamic loading. More recently, Carey[9] reported on gas-deployed skirt flutter studies using both finite element analyses and subscale cold-flow tests. The latter semiempirical/analytical studies, which were corroborated by subscale motor test firings, indicate a very stable, flutter-free design with a large flutter margin.

The objective of this study was to develop a general analytical tool for examining axisymmetric flutter of thin, conical shells with particular application to rocket nozzle exit cones. Simplifying assumptions applied herein include those of an isotropic material, uniform shell thickness, and axisymmetric geometry. Boundary conditions can be varied as desired.

The solution scheme is an application of the finite element method to the aeroelastic behavior of shells. Element matrices, from which system matrices are assembled, for a thin, truncated conical shell frustum are described herein. Novozhilov's shell theory was used to derive the element stiffness matrix. Shell stiffening by internal pressure was included via a geometric stiffness matrix. A consistent mass matrix was also obtained. For the aerodynamic matrices, linear piston theory was employed. Gasdynamic relations for a nozzle were developed by relating the dynamic pressure acting along the shell as a function of the rocket motor internal gas pressure and temperature.

The equation of motion for the shell structure was cast into standard eigenvalue form, and aeroelastic instability was deduced by tracking the real and imaginary parts of the eigenvalue as dynamic pressure was varied. The imaginary part corresponds to system frequency, while the real part corresponds to system damping. When the real part becomes positive, a perturbed motion increases exponentially corresponding to flutter.

The overall theory and procedure used in the present study are similar to that of Ueda and Kobayashi,[5] Bismarck-Nasr and Costa-Savio,[6] and Sunder et al.[7] They all used an axisymmetric conical shell frustum element. Important differences are noted in Table 1. The analysis reported by Carey[9] was based on a NASTRAN cyclic symmetry solution using triangular and quadrilateral membrane-bending plate finite elements. The inclusion of geometric stiffness was attempted without success. The axisymmetric shell element developed in this study and in Refs. 5-7 is not supported in NASTRAN aeroelastic analysis.

## Governing Equations

The general approach involved the use of an axisymmetric shell finite element with Fourier expansion to treat asymmetric response, thus allowing limited three-dimensional capability using a two-dimensional model. This approach is outlined in various references (e.g., Ref. 10) and is incorporated into several existing finite element structural analysis codes such as NASTRAN.[11]

The basic finite element considered was a simple conical shell frustum, Fig. 1. The neutral surface displacements $u$, $v$, and $w$ are functions of the independent variables $s$ and $\theta$. These deformations at any axial station may be expanded by a Fourier series of $m$ circular harmonics.

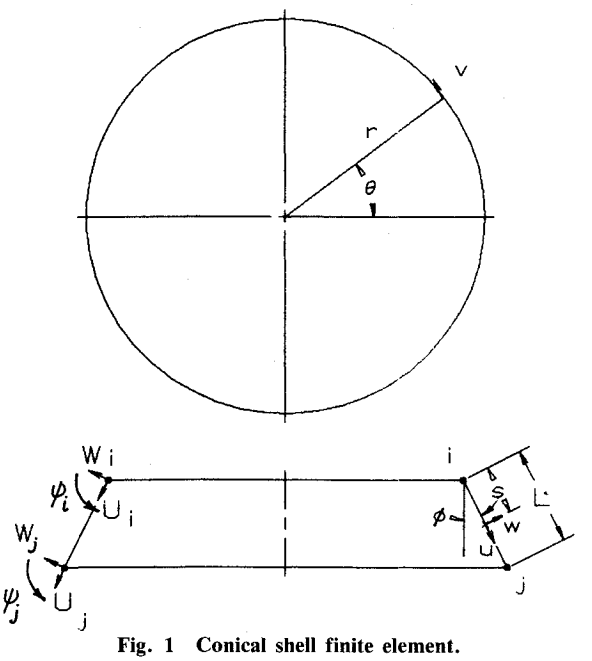


**Fig. 1 Conical shell finite element.**

**Table 1 Analysis comparison**

| | Present study | Ref. 5 | Ref. 6 | Ref. 7 |
|---|---|---|---|---|
| Shell theory | Novozhilov | Donnell | Novozhilov | |
| Two-dimensional quasisteady aerodynamics | With curvature correction | Yes | With curvature correction | Yes |
| Geometric stiffness | Yes | Yes | No | No |
| In-plane inertia | Yes | No | Yes | No |
| Material capability | Isotropic | Isotropic | Isotropic | Composite |
| Number of elements | 1-8 Higher-order elements | 10-20 with condensation | 10 | 11 with condensation |

$$\{u\} = \left[ [T_0] \ldots [T_n] \ldots [T_m] \right] \begin{Bmatrix} \{u_0\} \\ \vdots \\ \{u_n\} \\ \vdots \\ \{u_m\} \end{Bmatrix} \tag{1}$$

where

$$\{u_n\} = \begin{Bmatrix} u_n \\ v_n \\ w_n \end{Bmatrix}$$

and

$$[T_n] = \begin{bmatrix} \cos n\theta & 0 & 0 \\ 0 & \sin n\theta & 0 \\ 0 & 0 & \cos n\theta \end{bmatrix} \tag{2}$$

Shape functions relating the meridional displacement field throughout the element to displacements at the nodes are derived by assuming conventional shape functions[10] supplemented by higher-order shape functions, polynomials of sequentially increasing order written in the nondimensional body-centered variable and evaluated such that they exhibit zero displacements of the nodes (i.e., quadratic, cubic, etc.).

$$\{u\} = [N_1]\{U\} + [N_2]\{q\} = [N]\{U\} \tag{3}$$

where $\{U\}$ and $[N_1]$ are defined in Table 2 and $\{q\}$ and $[N_2]$ are defined in Table 3. The maximum number of generalized coordinates $\{q\}$ considered in Table 3 is 12 (four for each of the $u$, $v$, and $w$ displacements). The highest order polynomial shape function listed in Table 3 is of fifth order for the $u$ and $v$ deformations and of seventh order for the $w$ deformation.

The equation of motion of the $i$th degree of freedom was obtained via Lagrange's equation.

$$-\frac{\mathrm{d}}{\mathrm{d}t}\frac{\partial(\mathfrak{I}-u)}{\partial \dot{q}_i} + \frac{\partial(\mathfrak{I}-u)}{\partial q_i} = Q_i \tag{4}$$

The kinetic energy $\mathfrak{I}$ is

$$\mathfrak{I} = \frac{1}{2}\int_V \{\dot{u}\}^T[\rho]\{\dot{u}\}\mathrm{d}V \tag{5}$$

where $[\rho] = \rho_s[I]$.

The total strain energy $u$ is the sum of the strain energies associated with internal forces $u_i$ and that from initial stresses $u_g$. The strain energy $u_i$ is

$$u_i = \frac{1}{2}\int_V \{\sigma\}^T\{\epsilon\}\mathrm{d}V$$

Stresses are related to strains by

$$\{\sigma\} = [D]\{\epsilon\}$$

while strains are related to displacements by

$$\{\epsilon\} = [C]\{u\}$$

Substitution yields

$$u_i = \frac{1}{2}\int_V \{u\}^T[C]^T[D][C]\{u\}\mathrm{d}V \tag{6}$$

The strain-energy contribution $u_g$ for initial membrane forces resulting from circumferentially uniform internal pressure is[11]

$$u_g = \frac{1}{2}\int_V \{\omega\}^T[F_0]\{\omega\}\mathrm{d}V$$

where

$$[F_0] = \begin{bmatrix} N\theta_0 & 0 & 0 \\ 0 & Ns_0 & 0 \\ 0 & 0 & (Ns_0 + N\theta_0) \end{bmatrix}$$

and $N\theta_0$ and $Ns_0$ are membrane hoop and meridional forces for the zeroth harmonic, while $\{\omega\}$ are rotations related[11] to displacements by

$$\{\omega\} = [R]\{u\}$$

where

$$[R] = \begin{bmatrix} 0 & \frac{1}{r}\cos\theta & -\frac{1}{r}\frac{\partial}{\partial\theta} \\ 0 & 0 & \frac{\partial}{\partial s} \\ \frac{1}{2r}\frac{\partial}{\partial\theta} & -\frac{1}{2}\frac{\partial}{\partial s} + \frac{1}{r}\sin\theta & 0 \end{bmatrix}$$

**Table 2 Matrix $[N_1]$**

$$\begin{bmatrix} N_1(1,1) & 0 & 0 & 0 & N_1(1,5) & 0 & 0 & 0 \\ 0 & N_1(2,2) & 0 & 0 & 0 & N_1(2,6) & 0 & 0 \\ 0 & 0 & N_1(3,3) & N_1(3,4) & 0 & 0 & N_1(3,7) & N_1(3,8) \end{bmatrix}$$

where

$$N_1(1,1) = N_1(2,2) = 1-\xi$$
$$N_1(1,5) = N_1(2,6) = \xi$$
$$N_1(3,3) = 1 - 3\xi^2 + 2\xi^3$$
$$N_1(3,4) = L(\xi - 2\xi^2 + \xi^3)$$
$$N_1(3,7) = 3\xi^2 - 2\xi^3$$
$$N_1(3,8) = -L(\xi^2 - \xi^3)$$

and

$$\{U\} = \begin{Bmatrix} U_i \\ V_i \\ W_i \\ \psi_i \\ U_j \\ V_j \\ W_j \\ \psi_j \end{Bmatrix}$$

Substitution yields

$$u_g = \frac{1}{2}\int_V \{u\}^T[R]^T[F_0][R]\{u\}\mathrm{d}V \tag{7}$$

The work done by the aerodynamic forces is

$$w = -\int_A \frac{\rho v^2}{\sqrt{M^2-1}}\left(\frac{\partial w}{\partial s}+\frac{1}{v}\frac{(M^2-2)}{(M^2-1)}\frac{\partial w}{\partial t} - \frac{w}{2r\sqrt{M^2-1}}\right) w\mathrm{d}A$$

Let

$$w = [0\ 0\ 1]\begin{Bmatrix} u \\ v \\ w \end{Bmatrix} = [J]\{u\}$$

Substitution yields

$$w = -\int_A \rho v^2/\beta\{u'\}^T[J]^T[J]\{u\}\mathrm{d}A - \int_A \rho v(M^2-2)/\beta^3\{\dot{u}\}^T[J]^T[J]\{u\}\mathrm{d}A + \int_A \rho v^2/(2\beta^2)\{u\}^T[J]^T[J]\{u\}1/r\mathrm{d}A \tag{8}$$

Equation (1), when substituted into Eqs. (5-8), yields general energy and work expressions in terms of harmonic displacements. The equation of motion is then obtained by substitution into Eq. (4) and performing the integration which, after some manipulation, becomes

$$[m]\begin{Bmatrix} \ddot{U}_0 \\ \vdots \\ \ddot{U}_m \end{Bmatrix} + ([k]+[kg])\begin{Bmatrix} U_0 \\ \vdots \\ U_m \end{Bmatrix} = [a]\begin{Bmatrix} \dot{U}_0 \\ \vdots \\ \dot{U}_m \end{Bmatrix} + [b]\begin{Bmatrix} U_0 \\ \vdots \\ U_m \end{Bmatrix}$$

where, for instance,

$$[m] = \int_V [N]^T\begin{bmatrix} [T_0]^T \\ \vdots \\ [T_m]^T \end{bmatrix}[\rho]\Big[[T_0]\ldots[T_m]\Big][N]\mathrm{d}V$$

$$[m] = \int_V \begin{bmatrix} [N]^T[T_0]^T[\rho] & \cdots & [N]^T[T_0]^T[\rho] \\ \times[T_0][N] & & \times[T_m][N] \\ \vdots & & \vdots \\ [N]^T[T_m]^T[\rho] & \cdots & [N]^T[T_m]^T[\rho] \\ \times[T_0][N] & & \times[T_m][N] \end{bmatrix}\mathrm{d}V$$

Consider the $p$-$q$th partition of $[m]$,

$$\int_V [N]^T[T_p]^T[\rho][T_q][N]\mathrm{d}V = \int_L [N]^T\left(\int_0^{2\pi}[T_p]^T[\rho][T_q]\mathrm{d}\theta\right)[N]\mathrm{d}s$$

but

$$\int_0^{2\pi}[T_p]^T[\rho][T_q]\mathrm{d}\theta = 0, \quad p\neq q$$
$$= 0, \quad p=q$$

which produces the block diagonal matrix, each corresponding to an uncoupled harmonic.

The resulting uncoupled equations of motion for the $n$th circumferential harmonic are

$$[m_n]\{\ddot{\bar{U}}_n\} + ([k_n]+[kg_n])\{\bar{U}_n\} = [a_n]\{\dot{\bar{U}}_n\} + [b_n]\{\bar{U}_n\}$$

where

$$[m_n] = \int_V \{N\}^T[T_n]^T[\rho][T_n][N]\mathrm{d}V \tag{9}$$

which is the mass matrix for the $n$th circumferential harmonic. Similarly,

$$[k_n] = \int_V \{N\}^T[T_n]^T[C]^T[D][C][T_n][N]\mathrm{d}V = \int_V [B_n]^T[D][B_n]\mathrm{d}V \tag{10}$$

$$[kg_n] = \int_V [N]^T[T_n]^T[R]^T[F_0][R][T_n][N]\mathrm{d}V = \int_V [G_n]^T[F_0][G_n]\mathrm{d}V \tag{11}$$

$$[b_n] = -\rho v^2/\beta\int_A [N']^T[T_n]^T[J]^T[J][T_n][N]\mathrm{d}A + \rho v^2/(2\beta^2)\int_A [N]^T[T_n]^T[J]^T[J][T_n][N]1/r\,\mathrm{d}A = -\rho v^2/\beta\int_A [Nw]^T[Nw']\mathrm{d}A + \rho v^2/(2\beta^2)\int_A [Nw]^T[Nw]1/r\,\mathrm{d}A \tag{12}$$

$$[a_n] = -\rho v(M^2-2)/\beta^3\int_A [N]^T[T_n]^T[J]^T[J][T_n][N]\mathrm{d}A = -\rho v(M^2-2)/\beta^3\int_A [Nw]^T[Nw]\mathrm{d}A \tag{13}$$

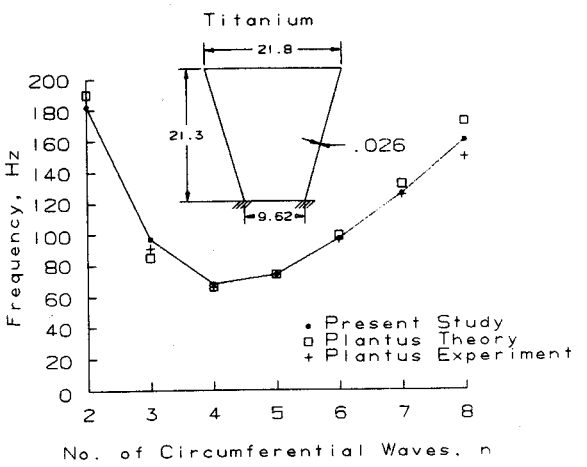


**Fig. 2 Conical shell frequency results.**

The aerodynamic terms are functions of local gas density, velocity, and Mach number, while the geometric stiffness is a function of the local pressure via the shell membrane forces. These local quantities, denoted by $i$, are related to gas properties in the chamber and to nozzle geometry.

$$\rho_i = (P_c/RT_c)(\rho/\rho_c)_i$$
$$v_i = \sqrt{g\gamma RM_i^2 T_c (T/T_c)_i}$$
$$P_i = P_c (P/P_c)_i \tag{14}$$

Over a narrow range of Mach numbers, $M$ is essentially a linear function of $\ell n(A/A^*)$. For $4.5 < M_i < 5.0$,

$$M_i = 0.66785(\ell n(A/A^*)_i + 2.4805) \tag{15}$$

From fundamental gas dynamic principles,[12]

$$(T/T_c)_i = \left(1+\frac{\gamma-1}{2}M_i^2\right)^{-1}$$
$$(\rho/\rho_c)_i = \left(1+\frac{\gamma-1}{2}M_i^2\right)^{-1/(\gamma-1)}$$
$$(P/P_c)_i = \left(1+\frac{\gamma-1}{2}M_i^2\right)^{-\gamma/(\gamma-1)} \tag{16}$$

Equation (15) can be substituted into Eqs. (16) and the result substituted into Eqs. (14) to obtain the local Mach number, density, velocity, and pressure.

The initial meridional and hoop membrane forces, $Ns_0$ and $N\theta_0$, are caused by pressure acting normal to the shell surface. The pressure varies with cone station as stated in Eqs. (14). Assuming a constant pressure between radii $r_i$ and $r_j$ [pressure $P$ at an average radius $r = \frac{1}{2}(r_i + r_j)$], then

$$N\theta_i = P_i r_i/\cos\theta$$
$$Ns_i = (r_j/r_i)Ns_j + [P/(2r_i\cos\theta)](r_j^2 - r_i^2)$$

where $Ns = 0$ at the free end.

## Solution Procedures

A general expression for the $n$th circumferential stiffness matrix was expressed in Eq. (10), where $[D]$ relates stresses to strains and $[B_n] = [C][T_n][N]$ relates strains to the $n$th circumferential nodal generalized displacements.

For an isotropic material, the material property matrix is

$$[D] = \frac{Eh}{1-\nu^2}\begin{bmatrix} 1 & \nu & 0 & 0 & 0 & 0 \\ \nu & 1 & 0 & 0 & 0 & 0 \\ 0 & 0 & (1-\nu)/2 & 0 & 0 & 0 \\ 0 & 0 & 0 & h^2/12 & \nu h^2/12 & 0 \\ 0 & 0 & 0 & \nu h^2/12 & h^2/12 & 0 \\ 0 & 0 & 0 & 0 & 0 & (1-\nu)h^2/24 \end{bmatrix}$$

Zienkiewicz[13] presented the Novozhilov[14] strain-displacement equations for a thin axisymmetric shell with nonsymmetric loading as

$$[C] = \begin{bmatrix} \frac{\partial}{\partial s} & 0 & 0 \\ \frac{1}{r}\sin\theta & \frac{1}{r}\frac{\partial}{\partial\theta} & \frac{1}{r}\cos\theta \\ \frac{1}{r}\frac{\partial}{\partial\theta} & -\frac{1}{r}\sin\theta + \frac{\partial}{\partial s} & 0 \\ 0 & 0 & -\frac{\partial^2}{\partial s^2} \\ 0 & \frac{1}{r^2}\cos\theta\frac{\partial}{\partial\theta} & -\frac{1}{r}\sin\theta\frac{\partial}{\partial s} - \frac{1}{r^2}\frac{\partial^2}{\partial\theta^2} \\ 0 & -2\sin\theta\cos\theta + \frac{2}{r}\cos\theta\frac{\partial}{\partial s} & \frac{2}{r^2}\sin\theta\frac{\partial}{\partial\theta} - \frac{2}{r}\frac{\partial^2}{\partial s\partial\theta} \end{bmatrix}$$

Equation (2) previously presented $[T_n]$ relating displacements to the $n$th circumferential displacements. The shape function matrix $[N]$ relates the $n$th circumferential displacements to the $n$th circumferential nodal-generalized displacements by

$$\{u_n\} = [N]\{U_n\}$$

The matrix $[N]$ was previously defined in Eq. (3) and Table 2. Integration of Eq. (10) was performed numerically using Simpson's rule with 12 steps over the element length.

Similarly, Eq. (9) gives the $n$th circumferential mass matrix. Equation (11) presents a general expression for the geometric stiffness matrix for the $n$th harmonic where

$$[G_n] = [R][T_n][N]$$

The $n$th circumferential aerodynamic stiffness and damping matrices were presented in general form in Eqs. (12) and (13) where $[Nw] = [J][T_n][N]$ and $[Nw'] = d([Nw])/ds$.

The system mass matrix, stiffness and geometric stiffness matrices, and aerodynamic damping and stiffness matrices are constructed by summing elemental matrices in the standard direct stiffness fashion. The equation of motion is then

$$[M_n]\{\ddot{U}_n\} + ([C_n] - [A_n])\{\dot{U}_n\} + ([K_n] - [B_n])\{U_n\} = \{0\}$$

which can be rearranged[15] to obtain

$$[D_n]\{y_n\} = \lambda_n[I]\{y_n\}$$

where

$$[D_n] = \begin{bmatrix} -[M_n]^{-1}([C_n] - [A_n]) & -[M_n]^{-1}([K_n] - [B_n]) \\ [I] & [0] \end{bmatrix}$$

A standard $QR$ eigensolver was used to perform the complex eigenvalue and eigenvector extraction.

## Validation Studies

Three thin conical shells, previously treated by various authors, were used as verification of the finite element techniques developed herein. The first problem considered was free vibration of a fixed-free cone. Finite element models of varying fidelity were studied to test element convergence and to establish an optimum model for subsequent studies. Second, a pressurized cone simply supported at both ends was examined to validate geometric stiffness effects. Finally, flut-

ter of a fixed-free cone subjected to an external supersonic flow was treated as validation of the aerodynamic effects.

Free vibration of a conical shell studied by Platus[16] and summarized by Leissa[17] was initially considered. This thin, conical, unpressurized shell, fixed at the smaller radius and free at the larger is shown in Fig. 2 along with dimensions, material properties, and plotted results. The lowest natural frequency, both analytically and experimentally, was reported by Plantus to be 66 Hz while vibrating in an $n=4$ circumferential wave pattern. In this study, higher-order shape function sets were assumed and used to supplement the basic ones as previously discussed. For the conical shell elements, the use of these additional functions increases the element matrix size upward from $8\times8$ depending on the number incorporated. To assess the effectiveness of using higher-order shape functions, the conical shell was modeled using varying numbers of uniformly spaced elements and varying numbers of higher-order shape functions. Figure 3 summarizes the lowest natural frequency calculated when using from 1 to 8 uniformly spaced elements and when using the basic shape functions plus from 0 to 4 higher-order shape function sets where each set is comprised of a $u$, $v$, and $w$ shape function. This figure demonstrates the convergence obtained as the number of elements are increased, using various numbers of higher-order shape function sets. The conical shell element convergence was improved more by the number of higher-order shape functions than by the number of elements (NE) used. For this case, the addition of only one set of higher-order shape functions ($p=1$) was quite effective.

Figure 2 compares NE = 4, $p=1$ predicted frequencies with those of Plantus for circumferential wave numbers up to $n=8$. Excellent agreement was obtained.

Weingarten[18] studied the vibration of a pressurized conical shell both analytically and experimentally. His specimen consisted of a thin aluminum cone simply supported at both ends so as to sustain an internal pressure (either positive internal pressure, $\Delta P/P_{amb}=+0.446$, or negative internal pressure, $\Delta P/P_{amb}=-0.446$). Cone dimensions and material properties are shown in Fig. 4 along with the NE = 4, $p=1$ finite element model assumed. Figure 5 summarizes the results and correlation of Weingarten's experimental results.

Shulman,[4] Dixon and Hudson,[2] Librescu,[19] Ueda and Kobayashi,[5] and Bismarck-Nasr and Costa-Savio[6] considered flutter of the conical shell shown in Fig. 6. This typical missile forward section is a thin conical shell fixed at both ends and subjected to external supersonic flow. Values of critical dynamic pressure parameter $P\nu^2R_1^3/(D\beta)$ ranging from 448 to 702 and $n=5$-6 were reported by the above authors using a variety of assumptions and techniques.

Figure 6 also shows the NE = 4, $p=1$ finite element model used in this study. In order to be consistent with the above investigators' initial assumptions, both material and aerodynamic damping, geometric stiffness, and aerodynamic curvature effects were ignored. The complex eigenvalues of the model were tracked as dynamic pressure (i.e., velocity) was varied. With an increasing dynamic pressure parameter, the imaginary parts of the first and second modes coalesced at a critical dynamic pressure parameter value of 562. At this value, the character of the first two roots changed from differing $\omega_1$ and $\omega_2$ with $\alpha=0$ to a pair of roots with imaginary ($\omega=\omega_1=\omega_2$) and real $\pm\alpha$ parts. The positive real part of the eigenvalue corresponds to the onset of flutter.

Figure 7 presents the present study results for $n=4$-7 compared to various other published results. The results of this

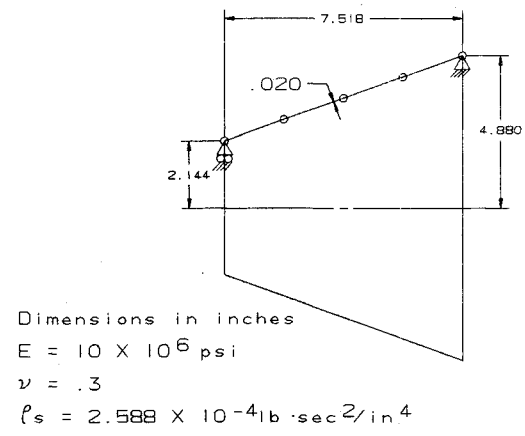


**Fig. 4 Simply supported conical shell model.**

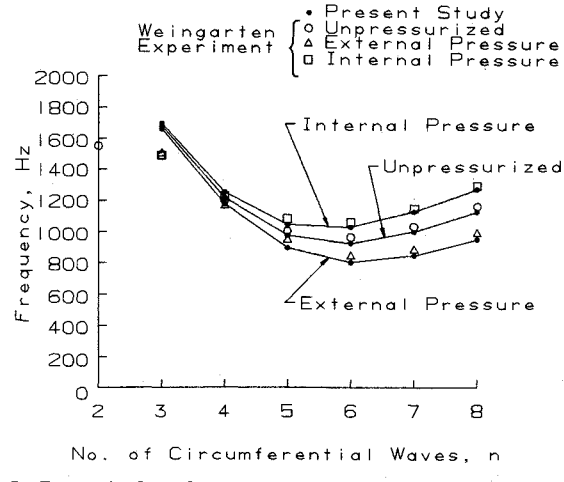


**Fig. 5 Pressurized and unpressurized simply supported conical shell frequency vs circumferential wave number.**

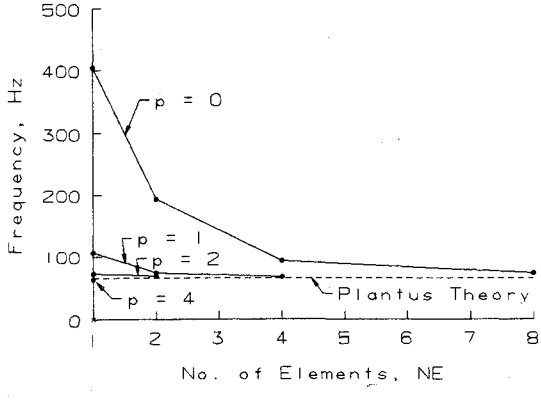


**Fig. 3 Frequency vs number of uniformly spaced elements and number of higher-order shape function sets.**

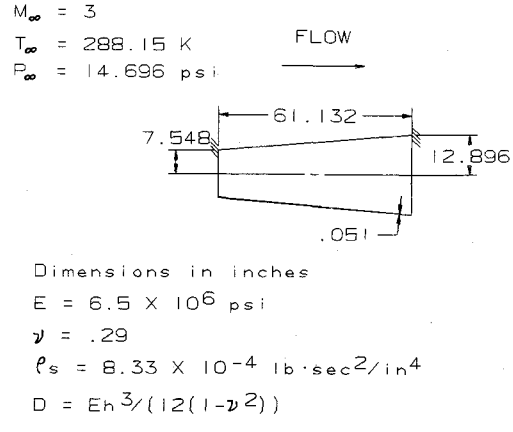


**Fig. 6 Conical shell flutter model.**

**Table 3 Matrix $[N_2]$**

$$\begin{bmatrix} N_2(1,1) & 0 & 0 & N_2(1,4) & 0 & 0 & N_2(1,7) & 0 & 0 & N_2(1,10) & 0 & 0 \\ 0 & N_2(2,2) & 0 & 0 & N_2(2,5) & 0 & 0 & N_2(2,8) & 0 & 0 & N_2(2,11) & 0 \\ 0 & 0 & N_2(3,3) & 0 & 0 & N_2(3,6) & 0 & 0 & N_2(3,9) & 0 & 0 & N_2(3,12) \end{bmatrix}$$

where

$$N_2(1,1) = N_2(2,2) = 1 + a_1\eta^2 \qquad a_1 = -4$$
$$N_2(1,4) = N_2(2,5) = \eta(1 + a_1\eta^2) \qquad b_1 = -8$$
$$N_2(1,7) = N_2(2,8) = 1 + c_1\eta^2 + c_2\eta^4 \qquad b_2 = 16$$
$$N_2(1,10) = N_2(2,11) = \eta(1 + c_1\eta^2 + c_2\eta^4) \qquad c_1 = -20$$
$$N_2(3,3) = 1 + b_1\eta^2 + b_2\eta^4 \qquad c_2 = 64$$
$$N_2(3,6) = \eta(1 + b_1\eta^2 + b_2\eta^4) \qquad d_1 = -46.16$$
$$N_2(3,9) = 1 + d_1\eta^2 + d_2\eta^4 + d_3\eta^6 \qquad d_2 = 321.28$$
$$N_2(3,12) = \eta(1 + d_1\eta^2 + d_2\eta^4 + d_3\eta^6) \qquad d_3 = -610.56$$

$$\{q\} = \begin{Bmatrix} q_{u1} \\ q_{v1} \\ q_{w1} \\ q_{u2} \\ q_{v2} \\ q_{w2} \\ q_{u3} \\ q_{v3} \\ q_{w3} \\ q_{u4} \\ q_{v4} \\ q_{w4} \end{Bmatrix}$$

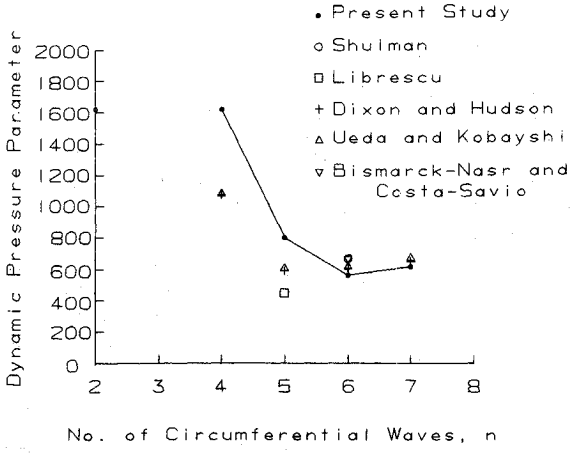


**Fig. 7 Conical shell flutter problem results comparison.**

study compare favorably with those of Dixon and Hudson[2] and Ueda and Kobayashi.[5]

In the preceding, aerodynamic damping and curvature effects were neglected. The results of including these effects are summarized in Table 4. Hence, aerodynamic damping was slightly stabilizing, while curvature was slightly destabilizing. The trend of these results is similar to those of Bismarck-Nasr and Costa-Savio.[6]

## Application

A proposed gas-deployed skirt (GDS) design, Fig. 8, was selected for evaluation. The GDS characteristics are given in Table 5.

As previously done on the conical shell validation problem, initially a free-vibration ($P_c = 0$) analysis was conducted. This indicated that the fundamental natural frequency occurs at $n = 20$ circumferential waves with a cantilever-like meridional shape.

The critical chamber pressure causing flutter was then determined for $n = 20$ to be $8000 < P_c < 8100$ psi. An unanticipated result was that two higher modes (modes 6 and 7), rather than the two lowest modes, coalesced to produce flutter. This behavior was initially disturbing for at least two reasons. First, it was presumed that flutter would occur in a circumferential wave pattern near that of the fundamental free-vibration mode ($n = 20$, in this case). Second, model accuracy in the sixth and higher modes is questionable simply due to model fidelity.

Sander et al.[20] reported a similar experience of higher mode coalescence. Hence, it was decided to investigate other circumferential wave numbers. Critical flutter chamber pressures were established for circumferential wave patterns be-

**Table 4 Aerodynamic damping and curvature effects**

| Effect considered | Dynamic pressure parameter for $n = 6$ |
|---|---|
| Neglect aerodynamic damping and curvature effects | 562 |
| Include curvature effects | 555 |
| Include aerodynamic damping and curvature effects | 571 |

**Table 5 GDS characteristics**

| | |
|---|---|
| Geometric variables: | |
| $R_1$ | 34.38 in. |
| $h$ | 0.016 in. |
| $(A/A^*)_1$[a] | 100 |
| $(A/A^*)_2$[b] | 131.45 |
| $\phi$ | 21.5 deg |
| Material variables: | |
| $E$ | $13 \times 10^6$ psi |
| $\nu$ | 0.38 |
| $\rho_s$ | 8.023 lb-s$^2$/in.$^4$ |
| Aerodynamic variables: | |
| $P_c$ | 575 psi |
| $T_c$ | 6220°R |
| $R$ | 640.2 |
| $\gamma$ | 1.18 |

[a] 1 = entrance station. [b] 2 = exit.

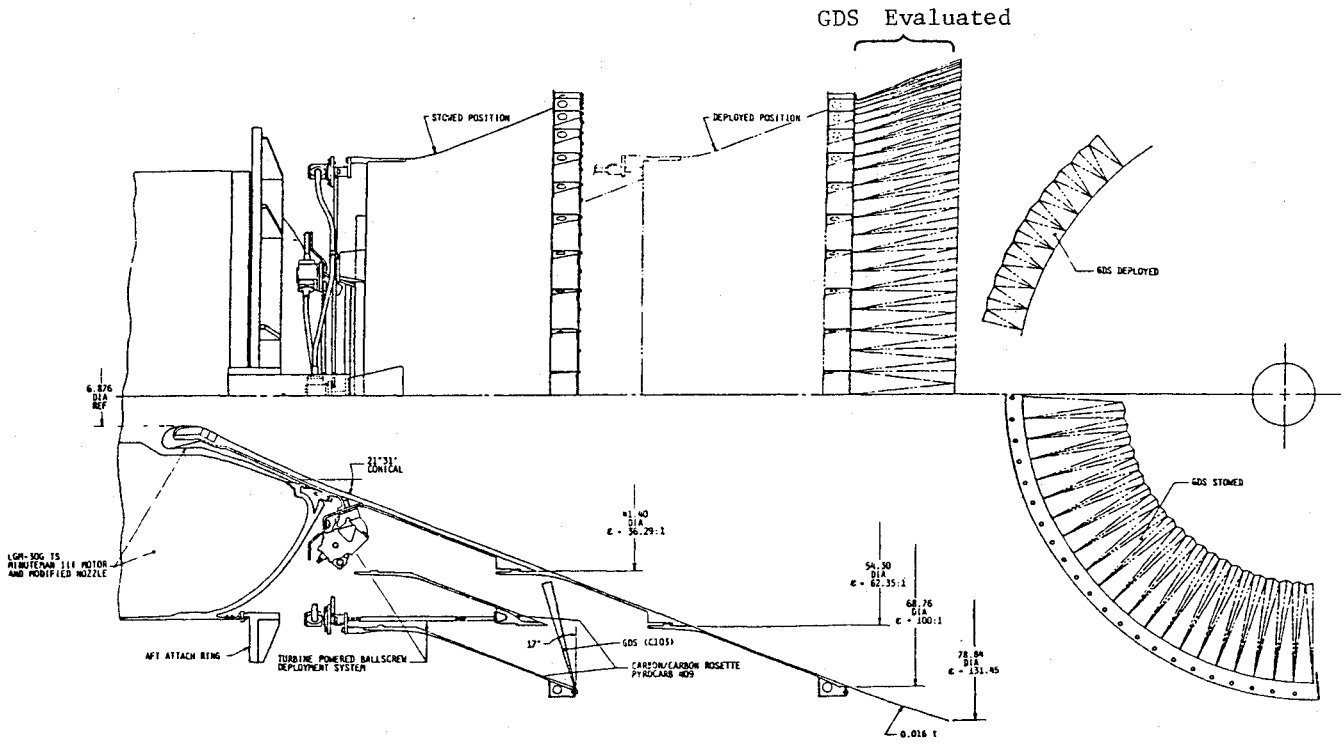


Fig. 8 Gas-deployed skirt design.

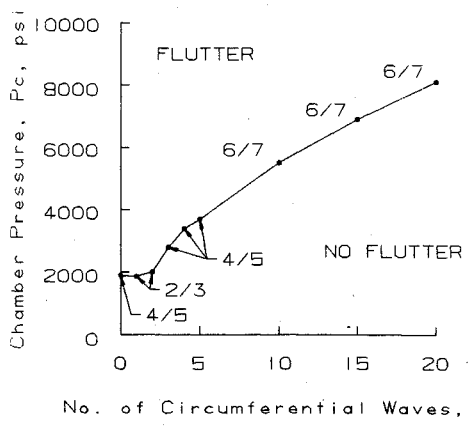


Fig. 9 Chamber pressure causing GDS flutter for various circumferential wave patterns.

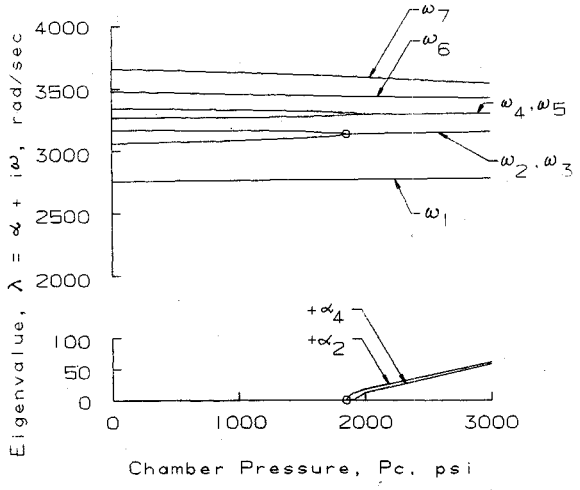


Fig. 10 GDS $n=1$ eigenvalue variation with increasing chamber pressure.

tween $0<n<20$. Results are plotted in Fig. 9. The lowest chamber pressure causing flutter was between 1850 and 1860 psi and occurred at $n=1$. Figure 10 maps, for $n=1$, the variation of real and imaginary eigenvalue parts with increasing chamber pressure and indicates a coalesence of modes 2 and 3. The numerals included above the data points in Fig. 9 note which modes coalesed. As the circumferential wave number was increased, coalescence shifted to higher modes as suggested by Sander et al.

For this problem, a flutter chamber pressure in excess of 1850 psi was well above the maximum expected operating pressure of the motor, hence a flutter margin in excess of 3 was predicted.

Although originally planned for a rocket motor static firing, this particular GDS was never tested. However, a subsequent GDS design was tested in 1983 on a motor designated IPSM-II DTM-3. For that design: $R_1=25.10$ in.; $h=0.012$ in.; $(A/A^*)_1=150$; $(A/A^*)_2=241.4$; $\phi=14.9$ deg; $E=13\times10^6$ psi; $\nu=0.38$; $\rho_s=8.023$ lb-s/in.; $P_c=647$ psi; $T_c=6092°$R; $R=640.2$; $\gamma=1.18$. A flutter chamber pressure in excess of 2400 psi was predicted, corresponding to a flutter margin of 3.7. No evidence of flutter was noted during the static firing.

Several other exit cone designs have been evaluated over the past several years. The effects of internal pressurization has a more stabilizing influence than originally anticipated. Often the flutter chamber pressure corresponds to a coalescence of higher-order meridional modes at higher-order harmonics. Large flutter margins have been calculated (and apparently demonstrated by virtue of successful motor static firings) for low expansion ratio, conventionally constructed exit cones typical of lower stage rocket motors. Several upper-stage motor applications, typified by thin, large diameter, often of carbon/carbon construction, exit cones or by GDS designs, have been predicted to flutter only at very thin wall thicknesses, much less than the design thickness. No actual motor firings of these designs have experienced flutter.

## Conclusions

An analytical tool was described herein based on the finite element method which, in general, treats the aerodynam-

ically induced flutter of conical shells and, in particular, treats axisymmetric flutter of rocket nozzle exit cones. Initially, the problem of rocket nozzle exit cone flutter was surveyed and applicable literature cited. The finite element was then introduced, appropriate energy relations manipulated to obtain the equation of motion, and stiffness, mass, and aerodynamic matrix relations were derived. Three problems were then considered as verification of the analytics. In these problems all parts were tested and validated, although no check problem is known that would verify all features acting in concert. A computer code was developed to specifically treat an isotropic, uniform thickness, conical shell frustum with internal supersonic flow. Finally, the program was applied to a typical rocket nozzle exit cone, gas-deployed skirt design. For this specific case, flutter was predicted to occur at a motor chamber pressure well above the design operating pressure—hence, the gas-deployed skirt was a stable design.

The technique outlined in this paper could be applied to more complicated situations such as a contoured nozzle with nonuniform wall thickness. Possible extensions include incorporating anisotropic material properties, composite shell relationships, rotatory inertia, and material damping.

At this point in time, there is a dearth of experimental data available as specific verification of this paper to rocket nozzle applications. Experimentally, all that is known is whether a given design did or did not experience flutter. Data concerning the few failures attributed to flutter range from sketchy and incomplete to nonexistent. Therefore, an organized cold-flow flutter test program on a family of thin conical shells is recommended to future investigators to fill this void.

## References

[1]Dixon, S. C. and Hudson, M. L., "Flutter, Vibration, and Buckling of Truncated Orthotropic Conical Shells with Generalized Elastic Edge Restraint," NASA TN D-5759, July 1970; also, supplement by same title.

[2]Dixon, S. C. and Hudson, M. L., "Supersonic Asymmetric Flutter and Divergence of Truncated Conical Shells with Ring-Supported Edges," NASA TN D-6223, May 1971.

[3]Miserentino, R. and Dixon, S. C., "Vibration and Flutter Tests of a Pressurized Thin-Walled Truncated Conical Shell," NASA TN D-6160, Feb. 1971.

[4]Shulman, Y., "Vibration and Flutter of Cylindrical and Conical Shells," MIT ASRL Rept. 74-2, OSR Tech. Rept. 59-776, June 1959.

[5]Ueda, T. and Kobayashi, S., "Supersonic Flutter of Truncated Conical Shells," *Transactions of the Japan Society of Aeronautics and Space Science*, Vol. 20, No. 47, April 1977, pp. 13-30.

[6]Bismarck-Nasr, M. N. and Costa-Savio, H. R., "Finite Element Solution of the Supersonic Flutter of Conical Shells," *AIAA Journal*, Vol. 17, Oct. 1979, pp. 1148-1150.

[7]Sunder, P. J., Ramakrishnan, C. V., and Sengupta, S., "Finite Element Analysis of 3-Ply Laminated Conical Shell for Flutter," *International Journal for Numerical Methods in Engineering*, Vol. 19, 1983, pp. 1183-1192.

[8]Davidson, D. L. and Gutsfield, K. D., "Altitude Performance Evaluation of a Rocketdyne Extendable Nozzle," AEDC-TR-67-160, Sept. 1967.

[9]Carey, L. F., "Gas Deployed Skirt (GDS) EEC Characterization Program," Bell Aerospace Textron, Buffalo, NY, Contract F04611-79-C-0045, Aug. 1982, pp. 106-135.

[10]Grafton, P. E. and Strome, D. R., "Analysis of Axisymmetric Shells by the Direct Stiffness Method," *AIAA Journal*, Vol. 1, Oct. 1963, pp. 2342-2347.

[11]MacNeal, R. H., ed., *The NASTRAN Theoretical Manual (Level 15.5)*, MacNeal-Schwendler Corp., MSR-40, May 1974, pp. 5.9.1-35, 7.4.1-7.

[12]Zucker, R. D., *Fundamentals of Gas Dynamics*, Matrix Publishers, Portland, OR, 1977, pp. 94-95.

[13]Zienkiewicz, O. C., *The Finite Element Method in Structural and Continuum Mechanics*, McGraw-Hill Publishing Co., Ltd., London, 1967, pp. 138-147.

[14]Novozhilov, V. V., *The Theory of Thin Shells*, P. Noordhoff Ltd., Groningen, the Netherlands, 1959, pp. 19-27.

[15]Hurty, W. C. and Rubinstein, M. F., *Dynamics of Structures*, Prentice-Hall, Englewood Cliffs, NJ, 1964, pp. 318-322.

[16]Platus, D. H., "Conical Shell Vibrations," NASA TN D-2767, April 1965.

[17]Leissa, A. W., "Vibration of Shells," NASA SP-288, 1973.

[18]Weingarten, V. I., "The Effect of Internal or External Pressure on the Free Vibrations of Conical Shells," *International Journal of Mechanical Science*, Vol. 8, 1966, pp. 115-124.

[19]Librescu, L., *Elastostatics and Kinetics of Anisotropic and Heterogeneous Shell-Type Structures*, Noordhoff International Publishers, Leyden, the Netherlands, 1975.

[20]Sander, G., Bon, C., and Geradin, M., "Finite Element Analysis of Supersonic Panel Flutter," *International Journal for Numerical Methods in Engineering*, Vol. 7, 1973, pp. 379-394.